Thermodynamics and Kinetics of Three Mg-H-V_N Complexes in Mg:GaN from Combined First-Principles Calculation and Experiment

Donghwa Lee,[1,*] Brandon Mitchell,[2] Y. Fujiwara,[3] and V. Dierolf[2]
[1]Lawrence Livermore National Laboratory, 7000 East Avenue L-413, Livermore, California 94550, USA
[2]Lehigh University, Physics Department, 16 Memorial Drive E, Bethlehem, Pennsylvania 18015, USA
[3]Osaka University, Division of Materials and Manufacturing Science, 2-1 Yamadaoka, Suita, Osaka 565-0871, Japan
(Received 23 December 2013; revised manuscript received 28 February 2014; published 20 May 2014)

An understanding of the formation and dissociation process of Mg-H defects in GaN is of paramount importance for high efficient GaN-based solid-state lighting. Through a combination of first-principle calculations and experimental observations, we find the existence of three types of Mg related centers forming different Mg-H-V_N complexes in Mg:GaN. Our study shows that the three different arrangements, which differ by the relative position of the H, determine the degree of acceptor passivation by changing their charge state from +3 to +1. The energetic study demonstrates that the relative stability of the defect complexes can vary with the location of the Fermi level, as well as thermal annealing and electron beam irradiation. The inclusion of a V_N is shown to produce an additional variance in optical spectra associated with Mg acceptor activation, resulting from changes in the defect configurations and charge states. Our study shows that these three Mg-H-V_N complexes are key components for understanding the Mg acceptor activation and passivation processes.

DOI: 10.1103/PhysRevLett.112.205501 PACS numbers: 61.72.uj, 71.15.Mb, 71.55.Eq, 78.55.Cr

The success of nitride-based light-emitting diodes and solid-state lighting devices that are replacing conventional lightbulbs, is based on the realization of *p*-type GaN. Magnesium (Mg) is the commonly used acceptor for attaining *p*-type conductivity [1]; however, the presence of hydrogen during organometallic vapor phase epitaxy and metal organic chemical vapor deposition growth electrically neutralizes the Mg acceptors by forming Mg-H complexes [2]. It is generally believed that the H electrically passivates the Mg acceptors as an interstitial (H_i) bonded to a neighboring nitrogen (N) atom [3]. It is well known that activation of the Mg acceptors can be achieved by either thermal annealing or low energy electron beam irradiation (LEEBI) [4–7].

Diverse experimental studies have reported enhanced *p*-type conductivity by changing growth methods, environmental conditions, and thermal history of the sample. Although the level of *p*-type conductivity is highly dependent on growth and postprocessing techniques, the physical origins of the enhanced conductivity are often attributed to the dissociation of the Mg-H complexes. Most studies on the activation of the Mg-H_i complex provide a clear understanding of the change in electrical properties, based on the dissociation model of a single Mg acceptor. On the other hand, the variation of optical properties associated with the activation process is still not quite understood. Moreover, the fact that considerable amounts of nitrogen vacancies (V_N) and Hs are present and may group together, is often neglected for simplicity [8,9]. A recent study reported the existence of two Mg related acceptors in Mg:GaN, based on photoluminescence (PL) measurements of acceptor-bound excitons [10]. It was revealed that one of the two Mg related centers is highly sensitive to both annealing and electron injection, and thus exists in a metastable state with high Mg concentration. In this Letter, we propose that there exist essentially three Mg related centers whose energetic preferences vary by growth and postgrowth conditions.

Several experimental studies have previously reported changes in the visible-range optical spectra under various treatments. Low intensity red emission observed in resistive Mg:GaN was no longer present after LEEBI treatment, but returned after annealing in an NH_3 ambient, above 600 °C. The recovered emission was destroyed after subsequent N_2 annealing and LEEBI [4]. Similarly, a decrease in the red luminescence was also observed with increasing Mg concentration [11,12]. It is evident that there may be a link between the acceptor activation and the change in optical luminescence, via the migration of H within the proximity of the Mg-V_N-N complex. Thus, a systematic study on Mg-H-V_N complex is performed in order to provide a clear understanding of the presence of different Mg-related centers and their influence on diverse properties during the acceptor activation and passivation processes in Mg:GaN. Our study reveals that the Mg-H-V_N complex is an essential component to understand the variation of electronic and optical properties in Mg:GaN.

In this study, accurate hybrid functional theory [13] is employed to clarify the behavior of Mg-H complexes. All the calculations are performed within the PBE0 functional [13], which mixes 28% of Hartree-Fock exchange into density functional theory (DFT) [14] as implemented in the

Vienna *ab initio* simulation package (VASP) code [15]. The bulk GaN system, constructed by 128 atom supercell and Monkhorst-Pack k-point sampling [16] with a grid of $2 \times 2 \times 2$, was used for the Brillouin zone integration. The climbing-image nudged elastic band method [17,18] is used for locating minimum energy pathways. Optical spectra are obtained from the time-dependent Kohn-Sham equation, in its linear-response formulation [19,20].

As a first step, we performed a thorough search for different arrangements of Mg_{Ga}-H_i-V_N complexes to identify energetically favorable defect configurations. This study found that the Mg_{Ga}-H_i complex tends to attract V_N along the z axis to form Mg_{Ga}-V_N pairs. Figures 1(a)–1(c) show three possible configurations of Mg_{Ga}-H_i complexes in the vicinity of the V_N depending on the relative position of hydrogen. The three energetically preferential locations of H_i are identified as (i) an interstitial between Mg_{Ga} and N close to the V_N (Mg1), (ii) sitting on the V_N site (Mg2), and (iii) an interstitial between Ga and N, but further away from the V_N (Mg3). While these three configurations are all stable, our study predicts that the optimal location of the H_i coincides with the charge state of the defect complex, where the equilibrium state of the Mg_{Ga}-V_N defect pair is $+2$ (Mg'_{Ga}-$V_N^{\cdot\cdot}$). Figures 1(d)–1(f) show the variation of the electron charge density, introduced by the presence H_i, for each of the three configurations. The variation was determined by subtracting the charge density of the Mg_{Ga}-H_i-V_N complex from the isolated charge densities of the Mg_{Ga}-V_N and the H_i. The blue isosurfaces represent the regions where the electron density has increased and the red surfaces represent regions of depletion. As can be seen from Figs. 1(d)–1(f), the electron density is transferred to H_i from the neighboring N sites. As a result, if the complex is deficient by one electron ($+3$), the Mg_{Ga} acceptor preferentially attracts a H_i to increase the electron density, and Mg1 will be favored. In this charge state, the complex is electrically neutral with the Mg_{Ga} acceptor being passivated. On the other hand, when excess electron charge is already present near the Mg_{Ga} ($+1$ configuration), it is unfavorable to have the additional charge that comes with the H_i close to the Mg_{Ga}. It will be favorable for the H_i to be further away from the Mg_{Ga} to diminish the local excess electron charge density, and, consequently, either Mg2 or Mg3 will be formed. In this charge state, the configurations are electrically active and act as Mg_{Ga} acceptors. These three complexes are similar to those proposed by Meyers *et al.* [21].

We further performed defect formation energy (DFE) calculations to identify the energetic preference of the three Mg centers as a function of Fermi energy. The DFEs are calculated by traditional Zhang-Northrup formalism [22]: $E^f = E_t^{\mathrm{def}} - E_t^{\mathrm{perf}} + \mu_{\mathrm{Ga}} + \mu_{\mathrm{N}} - \mu_{\mathrm{Mg}} - \mu_{\mathrm{H}} + q\mu_e + \Delta E_{\mathrm{corr}}$, where E_t^{def} and E_t^{perf} are the total energy of the defective and perfect system. Chemical potentials of Ga and Mg are calculated from the total energy of bulk metal, while the chemical potentials of N and H are obtained from the N_2 and H_2 gas. The electron chemical potential, the addition of valence band maximum (VBM) of the perfect GaN and variable Fermi level within the band gap, is considered to compensate for the variation of electrons in the system. Makov-Payne correction is applied to reduce the finite-size error from our calculation [23]. Differences in potential at a reference point are incorporated for potential alignment correction of the charged Mg centers [24]. Figure 2 shows the DFEs of three defect arrangements as a function of Fermi level; blue, red, and black lines represent the DFE of Mg1, Mg2, and Mg3 configurations, respectively. Our calculations predict that the Mg_{Ga}-H_i-V_N complex prefers to have a $+3$ charge under high Mg concentration (Fermi level close to the VBM). Consequently, the electrically

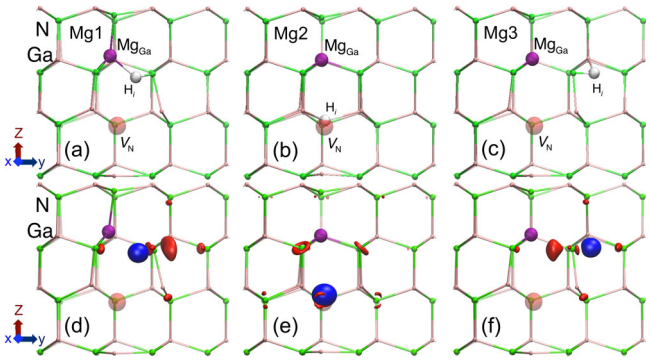

FIG. 1 (color online). Three different Mg_{Ga}-H_i-V_N configurations obtained from hybrid calculations: (a) Mg1, (b) Mg2, and (c) Mg3. (d)–(f) Variation of valence electron charge density due to the presence of hydrogen; each isosurface represents spatial distribution of accumulated (blue) and deficient (red) electronic charge density. The isosurfaces are plotted at $0.3e/\text{Å}^3$ (blue) and $-0.05e/\text{Å}^3$ (red). Each plot (d)–(f) corresponds to the configuration above it.

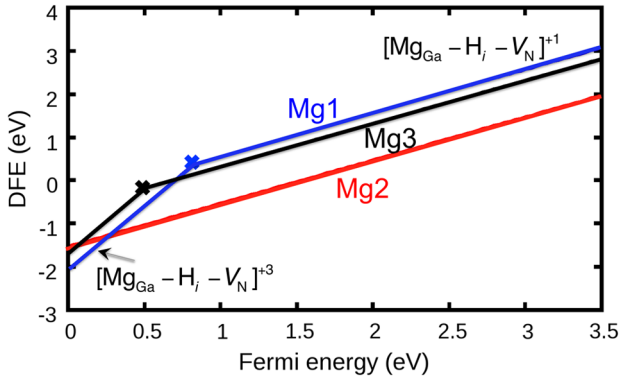

FIG. 2 (color online). Defect formation energy of Mg_{Ga}-H_i-V_N complex in Mg-doped GaN. Three different arrangements of the complex are shown as Mg1, Mg2, and Mg3. When the Fermi energy is close to 0 (valence band maximum, VBM), Mg1 is energetically favorable. With an increase in Fermi energy, Mg2 and Mg3 configurations become energetically more favorable than Mg1, and the preferential charge state on the complex is also changed from $+3$ to $+1$.

passivated Mg1 is energetically lower than Mg2 or Mg3 and low p-type conductivity is expected. As the Fermi level increases, a charge state of +1 becomes more favorable; see the change in the slope of Fig. 2. As a result, the electrically activated Mg2, which is energetically 1.06 eV lower than Mg1, becomes dominant. In addition, Mg3 can form rather than Mg1, since Mg3 is 0.25 eV lower in energy than Mg1, in the +1 charge state. Thus, the inversely proportional p-type conductivity of GaN at high Mg concentration is a result of the preferential formation of Mg1 over Mg2 as Fermi level approaches to VBM [25].

In a next step, we extend our study by exploring the migration process of the H_i. Since a diverse array of experimental studies have reported enhanced p-type conductivity after thermal and LEEBI annealing, it is important to understand the dynamics of H_i under these conditions. To this end, climbing image nudge elastic band calculations between the different configurations were performed [17,18]. Figure 3 shows the relative energy profile, along the migration pathway, from Mg1 to either Mg2 [Fig. 3(a)] or Mg3 [Fig. 3(b)]. Red lines show the energetics for the $[Mg_{Ga}\text{-}H_i\text{-}V_N]^{3+}$ state, while blue lines represent the energetics for the $[Mg_{Ga}\text{-}H_i\text{-}V_N]^{1+}$ state. In the +3 charge state, the migration process is endothermic with a high energy barrier so that Mg1 is preferred for both cases. As the configuration charge state is lowered from +3 to +1, the migration processes of the H_i change to exothermic with reduced energy barriers. For the movement of Mg1 to Mg2, the 3.45 eV energy barrier is significantly reduced to

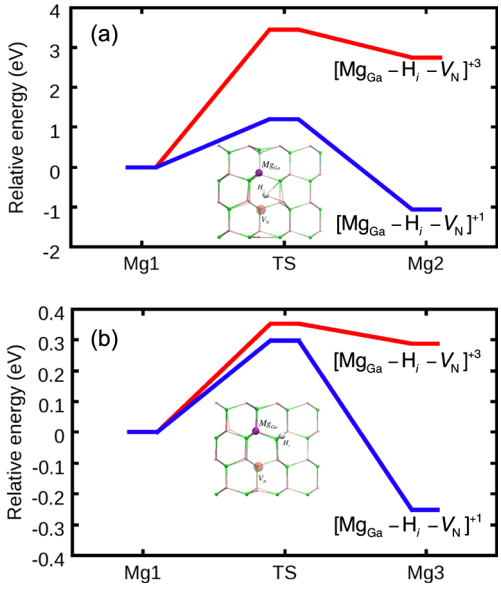

FIG. 3 (color online). Relative energy profiles along two hydrogen migration pathways: (a) Mg1 → Mg2 and (b) Mg1 → Mg3. Inset figures show the geometries at transition state. The change in charge states on the $Mg_{Ga}\text{-}H_i\text{-}V_N$ complex from +3 to +1 lowers the migration barrier and makes the migration exothermic. For both charge states, however, the Mg3 pathway is energetically more favorable. See the difference in energy scale.

1.21 eV. Similarly, the energy barrier for the migration from Mg1 to Mg3 is also reduced from 0.35 to 0.30 eV. Although the kinetic energy barriers for both migration pathways are lowered by the decrease in charge state, the barrier for Mg2 is still significantly higher than that for Mg3. As a result, temperature dependent activation processes are expected. At low temperature, the rate-limiting process for the migration is the energy barrier, and thus kinetically driven Mg3 formation will dominantly occur. At high temperature, the thermodynamically driven process will prevail and Mg2 will be primarily formed due to its energetic preference compared to Mg3. While the conversion from Mg1 to either Mg2 or Mg3 leads to acceptor activation, we find a strong temperature dependence for the underlying atomistic processes. These results are summarized in Table I.

Next, we compare these theoretical predictions with experimental observations. In this study, the Fermi-level dependence of the center formation is used to verify the thermodynamically driven center formation process. We studied a series of samples in which the Fermi level has been raised from its position close to the VBM, found in samples doped with Mg, by codoping with Si, while the Mg concentration (2.5×10^{19} cm^{-3}) is kept constant. For more information on the growth of these samples, see Ref. [26]. In order to identify the different complexes, we apply an approach that has been introduced in Ref. [27]. In this method, we use the emission of Eu^{3+} ions as a probe for the presence of the Mg1-3 complexes. To clarify the relation to the probe, these complexes are labeled Mg/Eu1-3 in Ref. [27]. We use the technique of combined excitation emission spectroscopy (CEES) in which the respective centers are resonantly excited. The resulting emission spectra give a measure of the relative abundance of the respective center. This technique also allows a distinction of the Mg1-3 centers from additional Si-related complexes that form as a result of the Si codoping.

Figures 4(a)–4(c) show CEES maps of three samples with (a) no Si, (b) medium Si (3.9×10^{18} cm^{-3}), and (c) high Si concentrations (7.9×10^{18} cm^{-3}). Black and white boxes outline the known spectral features from Mg1 and Mg2 centers, respectively. Starting with the sample without Si codoping, we find that Mg1 is predominantly formed [see Fig. 4(a)], as expected from Fig. 2. When Si was added, we find less Mg1 and an appearance of Mg2 [Fig. 4(b)]. The ratio of the integrated emission intensity of

TABLE I. Comparison on relative energetics along two migration pathways: Mg1 → Mg2 and Mg1 → Mg3. Two most energetically preferable states (+3 and +1) are considered.

	$[Mg_{Ga}\text{-}H_i\text{-}V_N]^{3+}$		$[Mg_{Ga}\text{-}H_i\text{-}V_N]^{1+}$	
	E_a	E_f	E_a	E_f
Mg1 → Mg2	3.45	2.74	1.21	−1.06
Mg1 → Mg3	0.35	0.29	0.30	−0.25

Mg1/Mg2, for this sample, is 2.6. As the Si concentration is further increased, the formation of Mg1 is further inhibited, while the formation of Mg2 is clearly enhanced [Fig. 4(c)]. For this sample, the intensity ratio is reduced to 1.6. Thus, our experimental study successfully verifies the Fermi level dependence of the preferential Mg complexes predicted from DFE calculations.

In regards to the activation dynamics, we find that Mg3 is not present in observable numbers in the as-grown samples, as expected from the fact that this complex is energetically less favorable than either Mg2 or Mg1, through the entire range of Fermi energy levels. In other words, thermodynamic processes mainly govern the formation of Mg centers in the as-grown samples. On the other hand, a previous study has shown that the intensity of Mg3 becomes significantly enhanced under low-temperature LEEBI treatment [27]. In this case, the center formation depends on the kinetic barrier of H_i migration as discussed above. This point was made even clearer in another study where UV irradiation at 10 K led to the formation of Mg3 alone, since the excess energy was not sufficient to form Mg2 [28]. In all, the experimental observations are consistent with our theoretical findings on the kinetics of the Mg-H complexes, in different temperature regimes.

Finally, since previous studies have reported the changes in luminescence under various treatments, we further perform linear response time-dependent DFT calculations to understand the effect of the H_i position on the optical properties of Mg:GaN [19,20]. Figure 5 shows the calculated optical spectra associated with three Mg centers. The calculations show that the change in the H_i position indeed modifies the UV and visible-range optical spectra. Two strong peaks, produced by Mg1 at 2.24 eV (yellow) and 3.27 eV (UV), are shifted to 2.01 eV (red) and 3.17 eV (UV) as the H moves to the second nearest interstitial site, forming Mg3. On the other hand, the formation of Mg2 reduces the emission within the visible range and one UV peak is only observed at 3.04 eV. Although these changes cannot be observed in our Eu-doped samples [29], other experimental studies have clearly shown the similar changes of luminescence under various treatments [4,10,11,30]. In particular, Monemar *et al.* have observed the redshift of MOCVD grown Mg:GaN by UV irradiation at 2 K [10]. Bayerl *et al.* have observed the quenching of visible luminescence by adding Si to MOCVD grown Mg:GaN samples [30]. Although Yan *et al.* have proposed the possibility of yellow and red luminescence associated with V_N, the study has neglected the additional variations coupled with the position of H_i [9]. Without the inclusion of H_i, the absence of red luminescence from MBE samples and quenching and returning of yellow and red luminescence cannot be explained [2,4,30]. Therefore, our DFT study shows that the three Mg_{Ga}-H_i-V_N complex are essential components for understanding the electrical and optical properties of Mg:GaN.

In conclusion, first-principle calculations are employed to shed light on the activation and passivation process of the Mg-H complex. Energetic studies showed three possible arrangements of the Mg_{Ga}-H_i-V_N complex depending on relative location of hydrogen. We have shown that the change in Fermi level will alter the preferential charge state of the defect complex, and thus controls the extent to which the Mg acceptors are passivated. We believe that the inclusion of V_N in many of the passivated complexes is

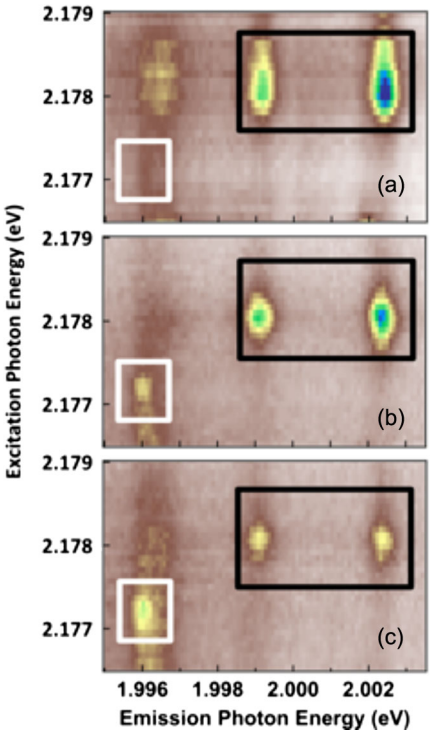

FIG. 4 (color online). Subsets of CEES maps that reveal the variations in the formation of Mg1 (black) and Mg2 (white) between GaN:Eu, Mg samples with increasing Si concentrations. (a) contains no Si, (b) had a lower Si concentration, and (c) had a higher Si concentration.

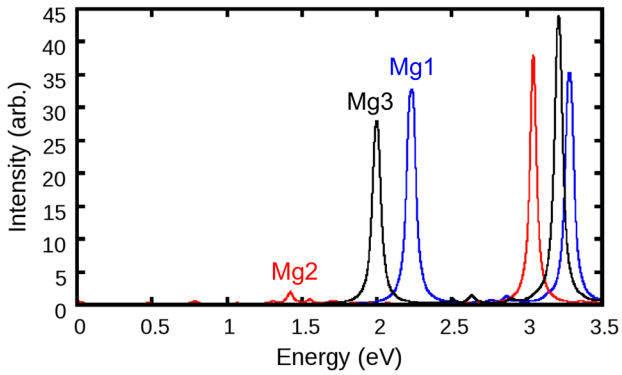

FIG. 5 (color online). Comparison of optical spectra calculated from three differently configured Mg_{Ga}-H_i-V_N complexes. Optical spectra are obtained by performing time-dependent DFT calculation on eigenstate obtained by PBE0 functional.

necessary, given their abundance and energetic favorability in Mg:GaN. Furthermore, the relative position of the H_i determines the electronic and optical properties of the V_N gap state during Mg acceptor activation process. The variance in defect arrangements is further confirmed by a novel experimental approach using Eu ions as a probe. Our investigations indicate that the formation of these complexes, and their associated acceptor passivation, is very sensitive to process parameters and suggests that further optimization may be possible by, e.g., using a combined approach, such as LEEBI under a lower thermal annealing temperature.

The experimental work performed by B. M. and V. D. was supported by NSF Grant No. ECCS-140038. The experimental work performed by Y. F. was supported by a Grant-in-Aid for Scientific Research (S) (Grant No. 24226009) from the Japan Society for the Promotion of Science. Part of the work was performed under the auspices of the U.S. Department of Energy by Lawrence Livermore National Laboratory under Contract No. DE-AC52-07NA27344.

*lee1004@llnl.gov

[1] H. Morkoç, *Handbook of Nitride Semiconductors and Devices: GaN-based Optical and Electronic Devices* (Wiley-VCH, Weinheim, 2008).
[2] S. Nakamura, N. Iwasa, M. Senoh, and T. Mukai, Jpn. J. Appl. Phys. **31**, 1258 (1992).
[3] J. Neugebauer and C. G. Van de Walle, Phys. Rev. Lett. **75**, 4452 (1995).
[4] S. Nakamura, T. Mukai, M. Senoh, and N. Iwasa, Jpn. J. Appl. Phys. **31**, L139 (1992).
[5] Y. Nakano, O. Fujishima, and T. Kachi, J. Appl. Phys. **96**, 415 (2004).
[6] Y. J. Lin, Appl. Phys. Lett. **84**, 2760 (2004).
[7] X. Li and J. J. Coleman, Appl. Phys. Lett. **69**, 1605 (1996).
[8] J. L. Lyons, A. Janotti, and C. G. Van de Walle, Phys. Rev. Lett. **108**, 156403 (2012).
[9] Q. Yan, A. Janotti, M. Scheffler, and C. G. Van de Walle, Appl. Phys. Lett. **100**, 142110 (2012).
[10] B. Monemar *et al.*, Phys. Rev. Lett. **102**, 235501 (2009).
[11] Y. Wei, Z. Xiao-Dong, Z. Li-Min, Y. Zhen, B. Hai, and L. Zheng-Min, Nucl. Instrum. Methods Phys. Res., Sect. B **264**, 41 (2007).
[12] S. Zeng, G. N. Aliev, D. Wolverson, J. J. Davies, S. J. Bingham, D. A. Abdulmalik, P. G. Coleman, T. Wang, and P. J. Parbrook, Appl. Phys. Lett. **89**, 022107 (2006).
[13] A. D. Becke, J. Chem. Phys. **98**, 5648 (1993).
[14] W. Kohn and L. J. Sham, Phys. Rev. **140**, A1133 (1965).
[15] G. Kresse and J. Furthmuller, Comput. Mater. Sci. **6**, 15 (1996).
[16] H. J. Monkhorst and J. D. Pack, Phys. Rev. B **13**, 5188 (1976).
[17] H. Jönsson, G. Mills, and K. W. Jacobsen, *Nudged Elastic Band Method for Finding Minimum Energy Paths of Transitions* (World Scientific, Singapore, 1998).
[18] G. Henkelman, B. P. Uberuaga, and H. Jonsson, J. Chem. Phys. **113**, 9901 (2000).
[19] M. E. Casida, in *Recent Advances in Density Functional Methods*, edited by D. P. Chong (World Scientific, Singapore, 1995), Vol. 1.
[20] S. Hirata and M. Head-Gordon, Chem. Phys. Lett. **314**, 291 (1999).
[21] S. M. Myers, A. F. Wright, M. Sanati, and S. K. Estreicher, J. Appl. Phys. **99**, 113506 (2006).
[22] S. B. Zhang and J. E. Northrup, Phys. Rev. Lett. **67**, 2339 (1991).
[23] G. Makov and M. C. Payne, Phys. Rev. B **51**, 4014 (1995).
[24] See Supplemental Material at http://link.aps.org/supplemental/10.1103/PhysRevLett.112.205501 for more details on computational methodology of defect formation energies.
[25] U. Kaufmann, P. Schlotter, H. Obloh, K. Kohler, and M. Maier, Phys. Rev. B **62**, 10867 (2000).
[26] D.-g. Lee, R. Wakamatsu, A. Koizumi, Y. Terai, and Y. Fujiwara, Jpn. J. Appl. Phys. **52**, 08JM01 (2013).
[27] B. Mitchell, D. Lee, D. Lee, A. Koizumi, J. Poplawsky, Y. Fujiwara, and V. Dierolf, Phys. Rev. B **88**, 121202 (2013).
[28] B. Mitchell, D. Lee, D. Lee, Y. Fujiwara, and V. Dierolf, Appl. Phys. Lett. **103**, 242105 (2013).
[29] A. Nishikawa, T. Kawasaki, N. Furukawa, Y. Terai, and Y. Fujiwara, Appl. Phys. Express **2**, 071004 (2009).
[30] M. W. Bayerl *et al.*, Phys. Rev. B **63**, 125203 (2001).